

Quadrupole-hexadecapole correlations in neutron-rich samarium and gadolinium isotopes

L. Lotina,^{1,2,*} K. Nomura,^{3,4,†} R. Rodríguez-Guzmán,^{5,‡} and L. M. Robledo^{2,6}

¹*Department of Physics, Faculty of Science, University of Zagreb, HR-10000 Zagreb, Croatia*

²*Departamento de Física Teórica and CIAFF, Universidad Autónoma de Madrid, E-28049 Madrid, Spain*

³*Department of Physics, Hokkaido University, Sapporo 060-0810, Japan*

⁴*Nuclear Reaction Data Center, Hokkaido University, Sapporo 060-0810, Japan*

⁵*Department of Physics, Nazarbayev University, 53 Kabanbay Batyr Ave., Astana 010000, Kazakhstan*

⁶*Center for Computational Simulation, Universidad Politécnica de Madrid, Campus de Montegancedo, Bohadilla del Monte, E-28660-Madrid, Spain*

(Dated: November 19, 2024)

We present an extensive study of quadrupole-hexadecapole correlation effects in even-even Sm and Gd isotopes with neutron number $N = 88 - 106$. The calculations are performed in the framework of the Gogny energy density functional (EDF) with the D1S parametrization and the *sdg* interacting boson model (IBM). The quadrupole-hexadecapole constrained self-consistent mean-field potential energy surface is mapped onto the expectation value of the *sdg*-boson Hamiltonian. This procedure determines the parameters of the *sdg*-IBM Hamiltonian microscopically. Calculated excitation energies and transition strengths are compared to the ones obtained with a simpler *sd*-IBM, as well as with the experimental data. The Gogny-EDF mapped *sdg*-IBM reproduces spectroscopic properties of the studied nuclei as reasonably as in the case of the previous *sdg*-boson mapping calculations that were based on the relativistic EDF, indicating that the axial quadrupole-hexadecapole method is sound regardless of whether relativistic or nonrelativistic EDF is employed. The mapped *sdg*-IBM improves some of the results in lighter Sm and Gd isotopes compared to the mapped *sd*-IBM, implying the existence of significant hexadecapole correlations in those nuclei. For those nuclei with $N \geq 94$, hexadecapole effects are minor, and the only significant difference between the two boson models can be found in the description of $E0$ monopole transitions.

I. INTRODUCTION

The importance of studying deformations in nuclei and their effects on various nuclear properties, e.g. excitation energies and transition strengths, has been recognized for decades [1, 2]. The most commonly present and extensively studied nuclear deformation is of quadrupole type, and their effects on the positive-parity states are well known. The higher-order correlations which affect the positive-parity states, the hexadecapole correlations, have been significantly less studied, due to their effects often being overshadowed by large quadrupole correlations. Nevertheless, the presence of hexadecapole correlations has been found in a wide range of nuclei [3, 4], and the main effect of such correlations is the appearance of the 4^+ band in the low-lying excitation energy spectra of some even-even nuclei, with an enhanced $B(E4)$ transition strength from the 4^+ band head state to the 0^+ ground state. Hexadecapole correlations have also been found to be important in describing certain nuclear reactions and decays. [4–6].

The interacting boson model (IBM) [7] is one of the most commonly employed models for studying how nuclear deformations affect low-lying spectra [8]. The main assumption of the model is that a nucleus can be ap-

proximated as a system consisting of a core, represented by the closest doubly-magic nucleus, and the valence nucleons, which form collective pairs (or bosons). Interactions among valence bosons give rise to the low-lying spectra and transitions. In the simplest version of the model, the *sd*-IBM-1, the nucleons primarily couple into s ($J^\pi = 0^+$) and d ($J^\pi = 2^+$) bosons, and the neutron and proton bosons are assumed to be identical [7]. One particular extension of the simple *sd*-IBM is the inclusion of g bosons ($J^\pi = 4^+$), allowing for the study of hexadecapole collectivity in nuclei. The importance of g bosons in describing low-lying collective states has been extensively studied [8–15]. In recent years, a method has been developed, which is to derive the parameters of the IBM Hamiltonian from self-consistent mean-field (SCMF) calculations based on a microscopic energy density functional (EDF) [16]. The method provides low-energy collective energy spectra and reduced transition probabilities, and has been successfully applied to study quadrupole [16–19], octupole [20, 21], and, recently, hexadecapole correlations [22, 23]. In this paper, we present an extension of Refs. [22, 23] by studying the low-energy quadrupole and hexadecapole collective states of even-even rare-earth isotopes $^{150-168}\text{Sm}$ and $^{152-170}\text{Gd}$, ranging from transitional to highly deformed nuclei, based on the Gogny force [24]. The present calculation employs parametrization D1S [25] of the Gogny interaction, which has already been extensively employed [26, 27]. The combination of the Gogny EDFs with the IBM through the mapping procedure has been considered and shown to be

* llotina.phy@pmf.hr; luka.lotina@uam.es

† nomura@sci.hokudai.ac.jp

‡ guzman.rodriguez@nu.edu.kz

valid to describe a number of nuclear structure phenomena, including coexistence of quadrupole shapes (e.g., Refs. [28, 29]) and octupole correlations (e.g., Refs. [30–33]).

Recently, Gogny Hartree-Fock-Bogoliubov (HFB) calculations were performed to compute potential energy surfaces (PESs) have been computed with constraints on the quadrupole and hexadecapole deformation parameters [34]. In this study, we carry out the mapping procedure by using the Gogny-D1S PESs in order to examine the effects of the quadrupole-hexadecapole coupling on the low-lying spectra of the considered nuclei. Since in previous studies [22, 23], calculations were performed within the framework of the constrained relativistic mean field (MDC-RMF) model [35, 36], with the relativistic density-dependent point-coupling (DD-PC1) functional [37, 38], this work will allow us to study how the quadrupole-hexadecapole mapping method depends on the choice of the EDF. On the other hand, we analyze positive parity bands in heavy Sm and Gd isotopes as well as the effects of hexadecapole collectivity in heavy neutron-rich nuclei, far from the valley of stability. The results of the calculations are compared with the ones obtained with a simpler *sd*-IBM, as well as with the available experimental data [39].

The paper is organized as follows. The theoretical framework, i.e., the Gogny-D1S HFB approach and the *sd*-IBM and *sdg*-IBM, is outlined in Sec. II. Potential energy surfaces computed with both SCMF and IBM calculations are presented in Section III. Spectroscopic properties, including the excitation spectra of low-lying states, electric quadrupole, hexadecapole, and monopole transition properties, are discussed in Sec. IV. Section V is devoted to the concluding remarks and work perspectives.

II. MODEL DESCRIPTION

In order to obtain the SCMF PES for the studied nuclei, the HFB equations have been solved with constraints on the axial quadrupole \hat{Q}_{20} and hexadecapole \hat{Q}_{40} moment operators [34]. The axial quadrupole $\beta_{20} \equiv \beta_2$ and hexadecapole $\beta_{40} \equiv \beta_4$ deformation parameters are related to the expectation values of the multipole moment operators as [34]:

$$\beta_\lambda = \frac{\sqrt{4\pi(2\lambda+1)}}{3R^\lambda A} \langle \hat{Q}_{\lambda 0} \rangle, \quad (1)$$

where $\lambda = 2$ or 4 , $R = 1.2A^{1/3}$ fm and A is the nucleon number. Details on the Gogny-D1S HFB calculations can be found in Refs. [25, 40, 41].

In order to calculate low-lying excitation energies and transition strengths, we have employed the *sdg*-IBM-1 model, referred to simply as *sdg*-IBM. The Hamiltonian is built in the same way as in Ref. [23]:

$$\hat{H} = \epsilon_d \hat{n}_d + \epsilon_g \hat{n}_g + \kappa \hat{Q}^{(2)} \cdot \hat{Q}^{(2)} + \kappa(1 - \chi^2) \hat{Q}^{(4)} \cdot \hat{Q}^{(4)}, \quad (2)$$

with $\hat{n}_d = d^\dagger \cdot \tilde{d}$ and $\hat{n}_g = g^\dagger \cdot \tilde{g}$ being the *d*- and *g*-boson number operators, respectively,

$$\hat{Q}^{(2)} = (s^\dagger \times \tilde{d} + d^\dagger \times s) + \chi \left[\frac{11\sqrt{10}}{28} (d^\dagger \times \tilde{d})^{(2)} - \frac{9}{7} \sigma (d^\dagger \times \tilde{g} + g^\dagger \times \tilde{g})^{(2)} + \frac{3\sqrt{55}}{14} (g^\dagger \times \tilde{g})^{(2)} \right] \quad (3)$$

being the quadrupole operator, and

$$\hat{Q}^{(4)} = s^\dagger \times \tilde{g} + g^\dagger \times s \quad (4)$$

being the hexadecapole operator. This Hamiltonian represents a modified version of the one used in Ref. [15], which satisfies the conditions of three symmetry limits: $[U(6) \supset U(5)] \otimes U(9)$, $SU(3)$ and $O(15)$ [42]. Here the quadrupole-quadrupole boson interaction is taken to be attractive, $\kappa < 0$, and a single *g* boson level is, to a good approximation, above that of a *d* boson, $\epsilon_d < \epsilon_g$. In addition, the requirement of the $SU(3)$ symmetry limit leads to the constraints that $-1 \leq \chi \leq +1$ and $-1 \leq \chi\sigma \leq +1$.

The parameters ϵ_d , ϵ_g , κ , χ and σ are determined by the mapping procedure [16]. The *sdg*-IBM is connected to the geometric model through a coherent state [43], $|\phi\rangle \sim (1 + \tilde{\beta}_2 d_0^\dagger + \tilde{\beta}_4 g_0^\dagger)^{N_B} |0\rangle$, with N_B representing the number of bosons, determined by the nearest doubly-magic nucleus, and $|0\rangle$ representing the boson vacuum. Note that $\tilde{\beta}_2$ and $\tilde{\beta}_4$ represent the axial bosonic quadrupole and hexadecapole deformation parameters, respectively. For Gd and Sm isotopes with $N < 106$, the core is represented by the doubly magic nucleus ^{132}Sn . In the case of ^{168}Sm and ^{170}Gd , the corresponding core is ^{176}Sn since the neutrons occupy the upper half of the neutron major shell $N = 82 - 126$.

The parameters of the *sdg*-IBM are fitted so that the PES of the IBM, $E_{\text{IBM}}(\tilde{\beta}_2, \tilde{\beta}_4) = \langle \phi | \hat{H} | \phi \rangle / \langle \phi | \phi \rangle$, should be approximately equal to the Gogny-HFB PES in the vicinity of the minimum:

$$E_{\text{SCMF}}(\beta_2, \beta_4) \approx E_{\text{IBM}}(\tilde{\beta}_2, \tilde{\beta}_4). \quad (5)$$

The relation between axial bosonic and fermionic parameters is assumed to be linear, $\tilde{\beta}_2 = C_2 \beta_2$, $\tilde{\beta}_4 = C_4 \beta_4$ as in previous studies with the mapping procedure [16, 21–23]. This leaves us with 7 parameters which need to be fitted to reproduce the SCMF PES.

For the *sd*-IBM calculations, we have employed the following Hamiltonian [7]:

$$\hat{H}_{sd} = \epsilon_d \hat{n}_d + \kappa \hat{Q}^{(2)} \cdot \hat{Q}^{(2)}, \quad (6)$$

where the *sd*-IBM quadrupole operator reads:

$$\hat{Q}^{(2)} = s^\dagger \tilde{d} + d^\dagger s + \chi (d^\dagger \times \tilde{d})^{(2)}. \quad (7)$$

The parameters ϵ_d , κ , χ in the *sd*-IBM Hamiltonian are fixed by a 1D mapping of the Gogny-D1S PES along the $\beta_4 = 0$ line:

$$E_{\text{SCMF}}(\beta_2, \beta_4 = 0) = E_{sd\text{-IBM}}(\tilde{\beta}_2), \quad (8)$$

and the relation between the bosonic and fermionic deformation parameters is assumed to be linear $\tilde{\beta}_2 = C_2^{sd}\beta_2$.

In order to calculate transition strengths with both the *sdg*-IBM and *sd*-IBM, the transition operators are constructed in the same way as in Refs. [22, 23]. The quadrupole transition operator is of the form:

$$\hat{T}(E2)_{sdg/sd} = e_2^{sdg/sd} \hat{Q}_{sdg/sd}^{(2)}, \quad (9)$$

with $\hat{Q}_{sdg/sd}^{(2)}$ representing the quadrupole operator of the *sdg* (3) or *sd* (7) boson model. The hexadecapole operator is chosen, in the case of *sdg*-IBM, to be:

$$\hat{T}_{sdg}^{(E4)} = e_4^{sdg} \left[s^\dagger \tilde{g} + g^\dagger s + (d^\dagger \times \tilde{d})^{(4)} \right], \quad (10)$$

while, for *sd*-IBM, it is constructed as:

$$\hat{T}_{sd}^{(E4)} = e_4^{sd} (d^\dagger \times \tilde{d})^{(4)}. \quad (11)$$

The quadrupole and hexadecapole effective charges $e_2^{sdg/sd}, e_4^{sdg/sd}$ are fitted in order to reproduce the measured transition strengths $B(E2; 2_1^+ \rightarrow 0_1^+)$ and $B(E4; 4_1^+ \rightarrow 0_1^+)$, from the first 2^+ and 4^+ states to the ground state 0^+ , respectively. The monopole transition operator [44] reads

$$\hat{T}_{sdg}^{(E0)} = (e_n N + e_p Z) \left(\eta \frac{\hat{n}_d}{N_B} + \gamma \frac{\hat{n}_g}{N_B} \right), \quad (12)$$

for the *sdg*-IBM, and

$$\hat{T}_{sd}^{(E0)} = (e_n N + e_p Z) \eta \frac{\hat{n}_d}{N_B}, \quad (13)$$

for the *sd*-IBM.

Following Ref. [44], we set neutron and proton effective charges to the values $e_p = e$ and $e_n = 0.5e$, while the values of parameters η and γ are taken to be $\eta = \gamma = 0.75 \text{ fm}^2$. Experimental data for energies and transition strengths have been taken from the NNDC database [39].

III. MAPPING THE SCMF RESULTS ONTO THE IBM SPACE

Figures 1 and 2 show the Gogny-D1S PESs obtained for even-even Sm and Gd isotopes with neutron numbers within the range $N = 88 - 106$, up to an energy of 2.7 MeV above the HFB ground state. The PESs for the $N = 106$ isotones are not shown due to their similarity to those of the $N = 104$ ones. As can be seen from the figures, the quadrupole and hexadecapole deformations associated with the absolute minima of the PESs start from the values $\beta_2^{\min} = 0.2$ and $\beta_4^{\min} = 0.08$, respectively. They increase with neutron number until $N = 94$, after which hexadecapole deformations start decreasing, dropping to $\beta_4^{\min} = 0.04$ at $N = 106$. Similar to previous (mapped) IBM calculations, based on the

relativistic DD-PC1 functional [22, 23], Sm isotopes exhibit larger HFB ground state β_4 values as compared to Gd isotopes. On the other hand, the ground state β_2 deformations increase up to $N = 94$. For larger neutron numbers, those quadrupole deformations decrease, reaching the value $\beta_2^{\min} = 0.32$ for $N = 106$ isotopes. An important thing to observe is that the PESs appear to be "tilted" with respect to β_{20} and β_{40} axes, indicating a strong coupling between the axial quadrupole and hexadecapole degrees of freedom, which has already been discussed in Ref. [34]. Note, that the results obtained for $N = 88 - 96$ isotopes agree well with the ones obtained with the DD-PC1 EDF [22, 23].

The corresponding (mapped) *sdg*-IBM PESs are depicted in Figs. 3 and 4. The mapping procedure reproduces basic features of the fermionic PESs such as the position of the absolute minima, the oblate saddle points for $N = 88$ nuclei as well as the overall shape of the surface. The strong quadrupole-hexadecapole coupling is well reproduced in $N \leq 100$ isotopes, while in $N > 100$ isotopes, the coupling is predicted to be less strong. Note that the IBM PESs are significantly flatter than the HFB ones, due to the restricted boson (valence) space as compared to the Gogny-HFB model space. This also explains why the mapping procedure is not able to reproduce the "elongated" shapes of the PESs for $N \geq 100$ nuclei. The 1D *sd*-IBM mapping has also been carried out in all the studied isotopes to reproduce some of the properties of the $E_{\text{SCMF}}(\beta_2, \beta_4 = 0)$ curve such as the position of the absolute minimum, the position and energy of the oblate saddle point, and the energy of the spherical $\beta_2 = 0$ configuration.

The *sdg*- and *sd*-IBM parameters are shown in Figs. 5 and 6, as functions of the neutron number N . The *d*-boson energy ϵ_d has a very similar behaviour in both models. It decreases up to $N = 100$, after which it stops decreasing, and even increases at $N = 106$, which corresponds to lower β_2^{\min} values. Moreover, the parameters κ , χ and C_2 also display a similar behaviour in both models, whereas in the *sdg*-IBM the χ parameter is characterized by significantly lower absolute values, compared to the *sd*-IBM ones. Regarding those parameters appearing only in the *sdg*-IBM, the *g*-boson energy ϵ_g takes values between $\epsilon_g = 1.1$ and $\epsilon_g = 1.3$ MeV. The C_4 parameter decreases until $N = 96$, after which it starts to increase, which corresponds to β_4^{\min} values becoming lower for $N \geq 96$ isotopes. Finally, with increasing neutron number, the parameter σ , which accounts for the quadrupole-hexadecapole coupling in the *sdg*-IBM, drops from $\sigma = 2.8$ to $\sigma = 1.0$, which also corresponds to a decrease in β_4^{\min} . This explains why the coupling is predicted to be less strong in $N > 100$ isotopes by the *sdg*-IBM. It should also be noted that σ decreases faster in Gd isotopes, compared to the Sm ones, which can be explained from the fact that β_4^{\min} values are smaller in Gd isotopes with the same N .

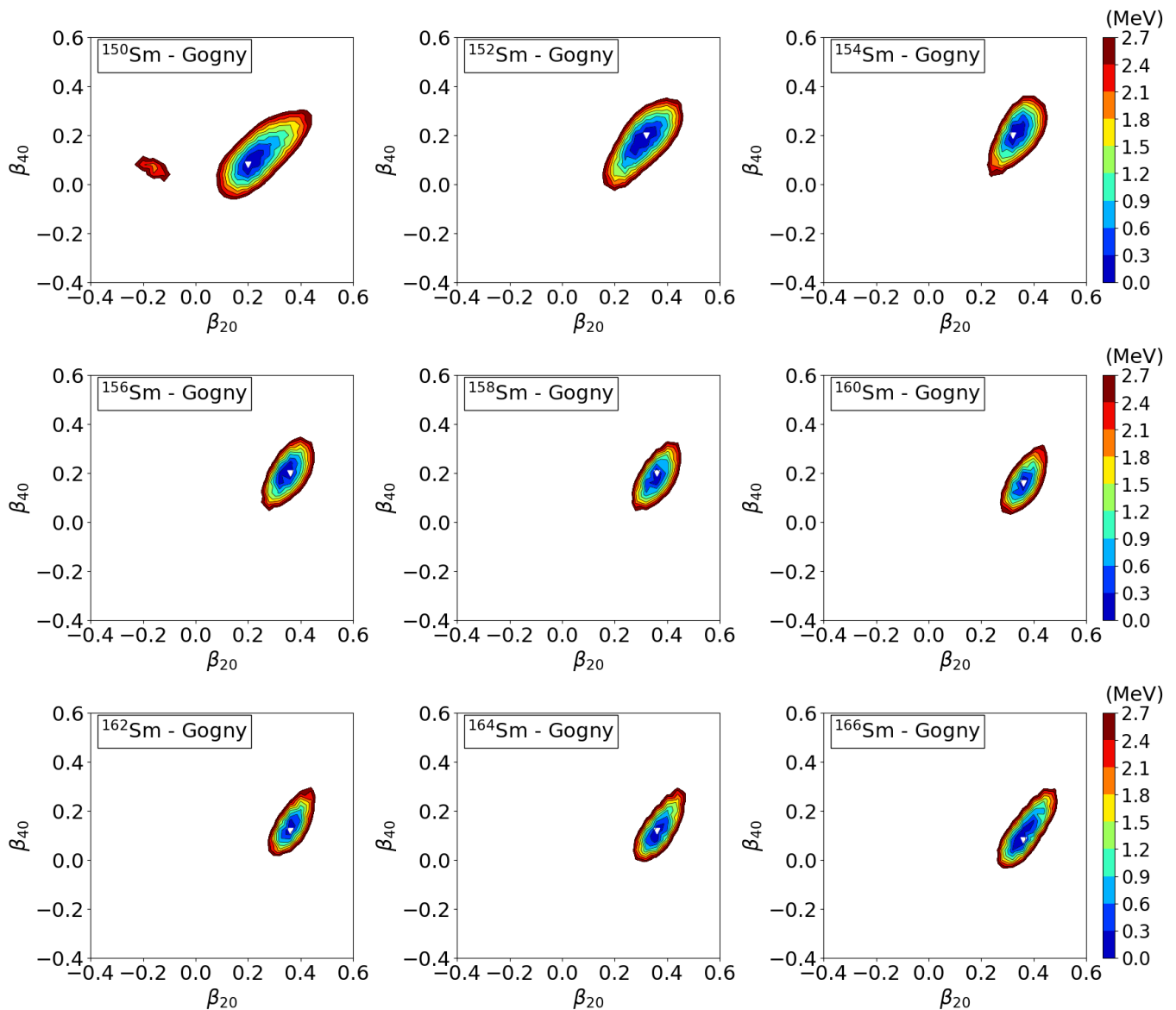


FIG. 1. Axially-symmetric quadrupole (β_{20}) and hexadecapole (β_{40}) constrained potential energy surfaces for $^{150-168}\text{Sm}$. The energy difference between neighbouring contours is 0.1 MeV. The absolute minimum is indicated by an open triangle. Results have been obtained with the Gogny-D1S energy density functional.

IV. RESULTS OF THE SPECTROSCOPIC CALCULATIONS

In this section, we discuss the excitation energies and transition strengths obtained from the diagonalization of the IBM Hamiltonian, using the computer program ARBMODEL [45]. The results of the *sdg*-IBM and *sd*-IBM will be compared to illustrate the effects of *g* bosons. The results obtained from both models will also be compared with the available experimental data at NNDC [39].

A. Excitation energies

Figure 7 shows the excitation energies corresponding to the yrast band states with even spin $J^\pi = 2^+$ to 14^+ . As expected, the *sdg*-IBM improves the description of the excitation energies of higher-spin states with $J^\pi = 12^+$ and 14^+ in transitional $N = 88$ nuclei. For Sm nuclei, the *sdg*-IBM gives a better description of the energy levels up to $N = 92$ than the *sd*-IBM. This can be explained by the fact that large amounts of *g*-boson contributions are present in the higher-spin states, as indeed, the expectation value of the *g*-boson number operator $\langle \hat{n}_g \rangle$ is greater or equal to 1 in those isotopes with $N \leq 92$.

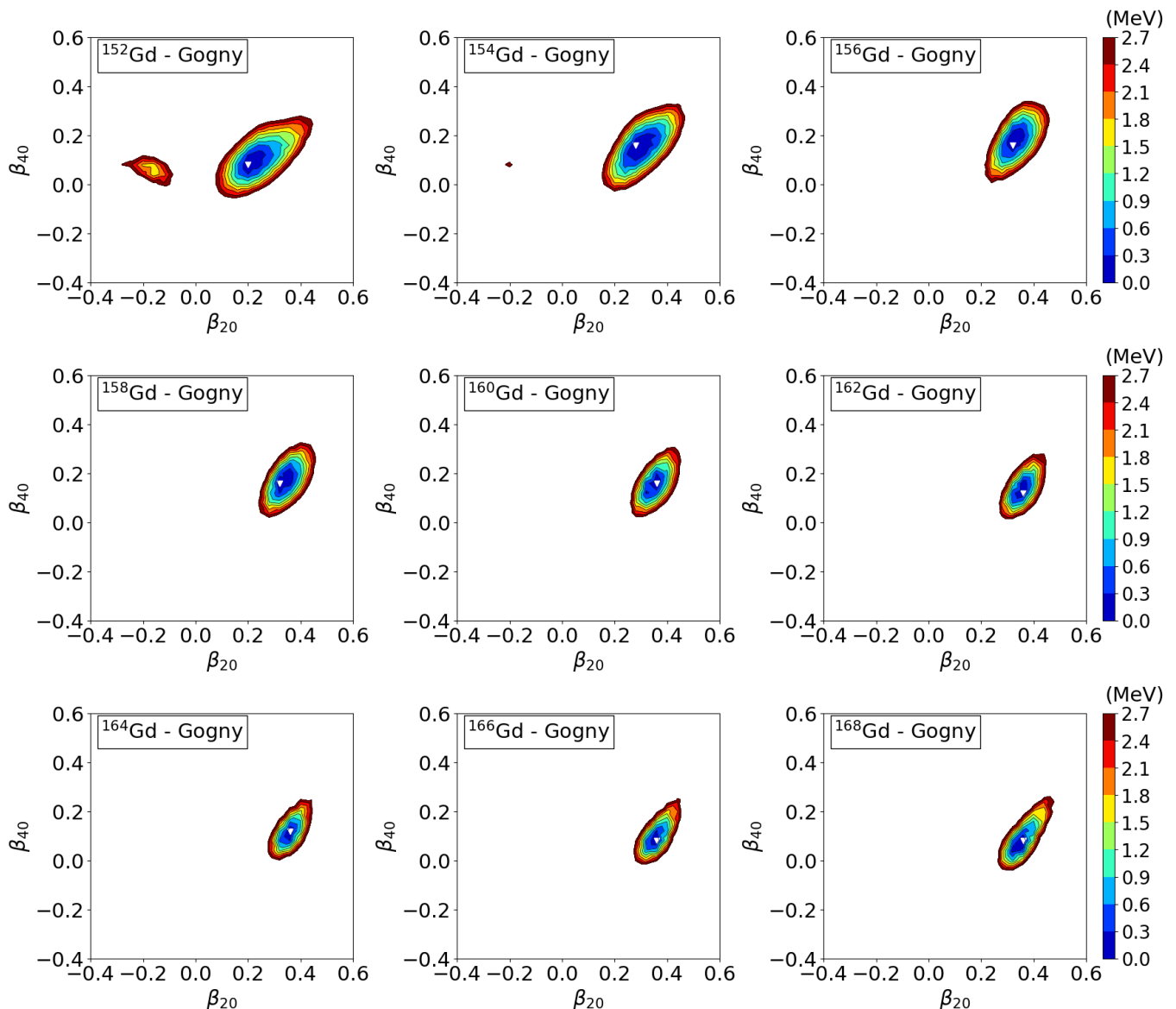


FIG. 2. The same as in Fig. 1, but for $^{152-170}\text{Gd}$.

Note that for Sm isotopes with $N \leq 92$, the β_4^{\min} values are larger compared to those for Gd isotopes with the same N . For the $N > 92$ isotopes, there is no significant difference between both models concerning the description of the ground state bands. This is not surprising, since as the number of valence nucleons increases for deformed nuclei even the sd -IBM is good enough to provide an accurate description of the yrast-band levels. In any case, in general the sdg -IBM does provide some significant improvements in the description of the yrast band, compared to the simpler sd -IBM.

Figure 8 depicts the excitation energies of the 0_2^+ , 2_3^+ and 4_3^+ states, which are associated with the $K^\pi = 0^+$ band in the present study. The sdg -IBM predicts a significantly low-lying 4_3^+ level for $N = 88$ isotopes. This

agrees better with the experimental data than in the corresponding sd -IBM results. For other isotopes, there is no significant difference between the two models, as they both predict similar energies for all three states. Overall, the sdg -IBM does not improve the description of the 0^+ band significantly.

Figure 9 shows the excitation energies of the 2_2^+ , 3_1^+ , and 4_2^+ states, which can be identified as members of the γ -vibrational band in the present calculation. Both models predict similar energies for Sm and Gd isotopes. Those energies mostly agree well with the experimental data. The description of the γ -vibrational band could be improved by including both three-body terms [19] and the γ degree of freedom at the HFB level. However, such an extension is beyond the scope of this paper. Work

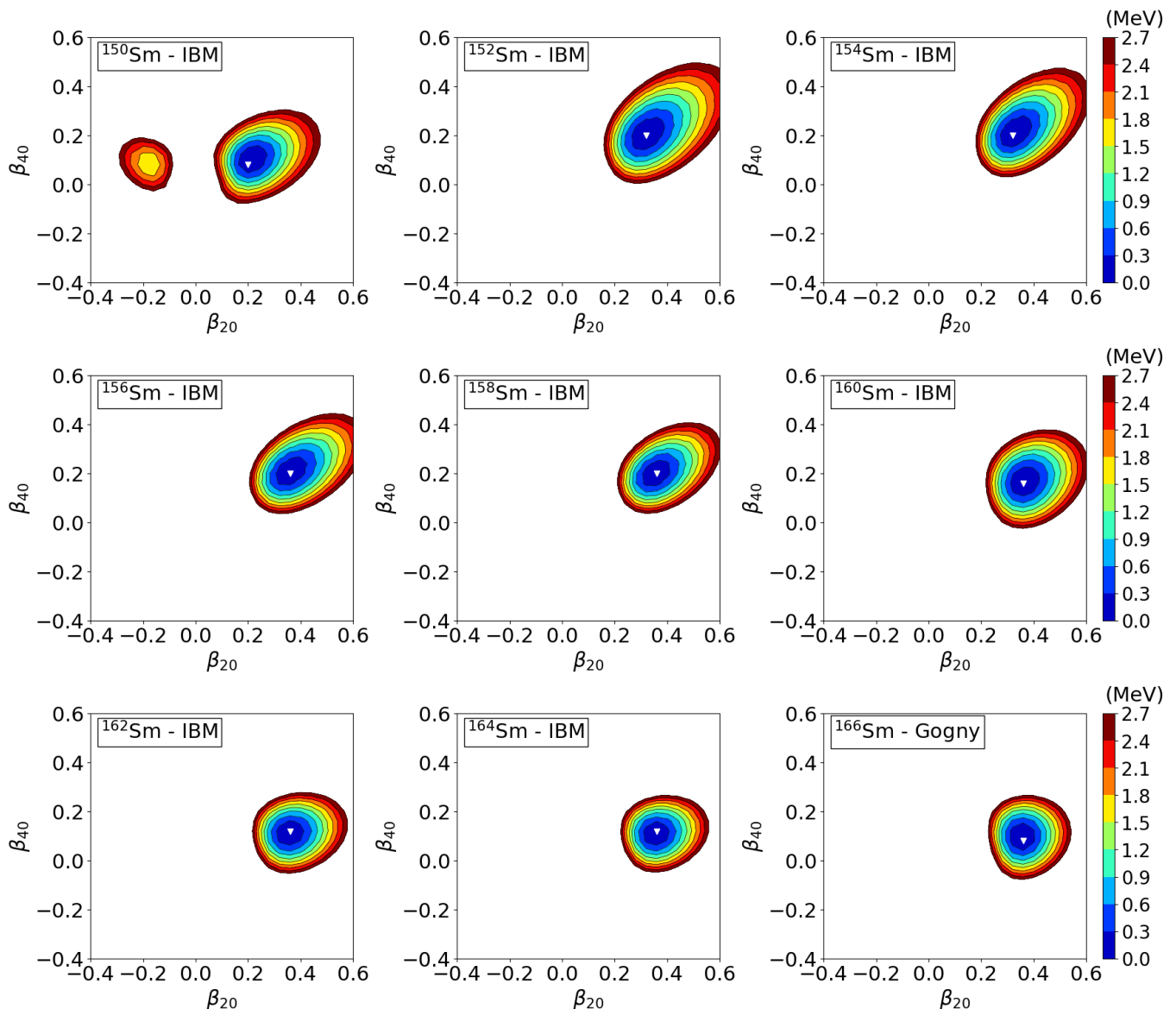


FIG. 3. The same as in Fig. 1, but for the mapped *sdg*-IBM potential energy surfaces of $^{150-168}\text{Sm}$.

along these lines will be reported in future publications.

B. Transition strengths

1. $E2$ transitions

Figure 10 shows the $B(E2; J \rightarrow J - 2)$ transition strengths in the ground state bands of the well deformed $N = 90$ and 92 isotones. These nuclei are specifically considered, since there are experimental data on $E2$ transitions. In Sm isotopes, the *sdg*-IBM significantly improves the description of $B(E2)$ transition strengths for $J^\pi \geq 6^+$. However, for ^{154}Gd , the *sdg*-IBM predicts $B(E2)$ strengths significantly larger than the *sd*-IBM,

which are however still smaller than the measured values. The discrepancy points towards some missing correlations other than the hexadecapole ones, that could also contribute to the $B(E2)$ strengths. Due to the large experimental error bars, in ^{156}Gd it is not possible to conclude whether *sdg*-IBM improves the description of the $E2$ transitions in the yrast band or not. The fact that the *sdg*-IBM predicts larger $B(E2)$ transition strengths than the *sd*-IBM can be attributed to the large values of the parameter σ (see Fig. 5). In the case of $^{152,154}\text{Sm}$ and ^{154}Gd the value $\sigma = 2.8$ leads to a significant contribution to the $B(E2)$ transition strengths arising, from the $[d^\dagger \times \tilde{g} + g^\dagger \times \tilde{d}]^{(2)}$ part of the quadrupole $\hat{Q}^{(2)}$ operator of Eq.(3). Moreover, the $\sigma = 2.1$ value obtained

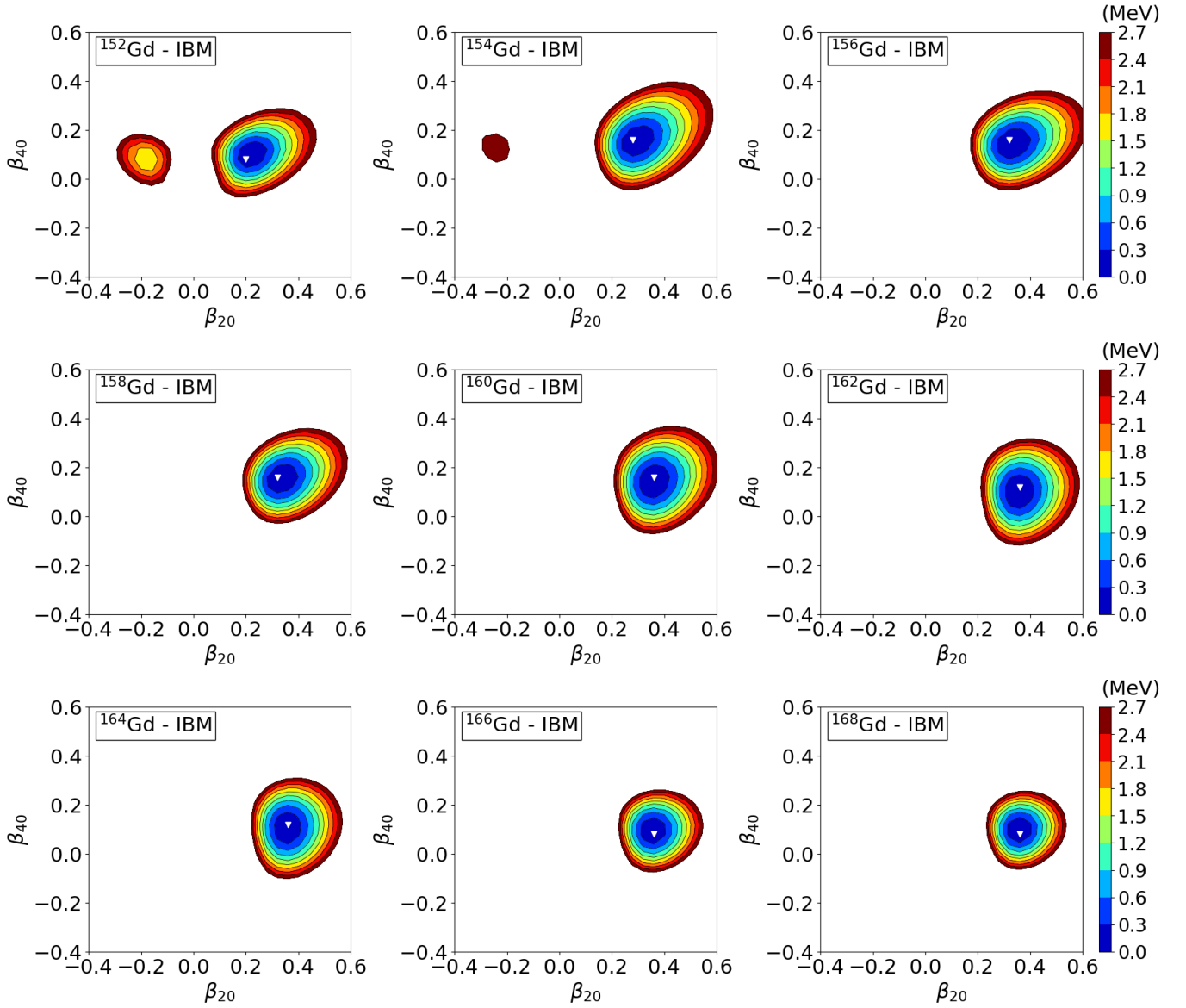


FIG. 4. The same as in Fig. 1, but for the mapped *sdg*-IBM potential energy surfaces of $^{152-170}\text{Gd}$.

for ^{156}Gd leads to similar *sdg*-IBM and *sd*-IBM $B(E2)$ strengths. Note that the σ values for $^{154,156}\text{Gd}$ are larger than those previously obtained [23] using microscopic input from the relativistic DD-PC1 EDF.

2. Hexadecapole transitions

The $B(E4; 4_n^+ \rightarrow 0_1^+)$ ($n = 1, 2, 3, 4$) reduced transition probabilities obtained in the mapped nucleon numbers are plotted in Fig. 11, as functions of the nucleon number A in order to avoid overlapping between the data for Sm and Gd isotopes. The $e_4^{sdg/sd}$ effective charges are fitted to the experimental $B(E4; 4_1^+ \rightarrow 0_1^+)$ values [39, 46–48]. Results for $B(E4; 4_1^+ \rightarrow 0_1^+)$ strengths are plotted

in panels (a) and (b) of the figure, while $B(E4)$ values from non-yrast 4_n^+ (with $n = 2, 3, 4$) to the 0_1^+ ground states are shown in panels (c)-(h). The 4_2^+ state typically belongs to the γ -vibrational band, where g bosons do not play a significant role. Thus both models predict weak $E4$ transitions in this case. Large *sdg*-IBM $B(E4)$ values are obtained for the 4_3^+ states in ^{150}Sm and ^{152}Gd . The strong $E4$ transition, predicted for the 4_4^+ state in ^{154}Gd , agrees well with the experimental identification of this state as a band head of the $K = 4^+$ band [39]. On the other hand, the *sd*-IBM gives negligibly small $B(E4)$ reduced transition probabilities. This indicates a significant difference between the *sdg*-IBM and the simpler *sd*-IBM. Nevertheless, experimental data on $B(E4)$ strengths in rare-earth nuclei are still required to under-

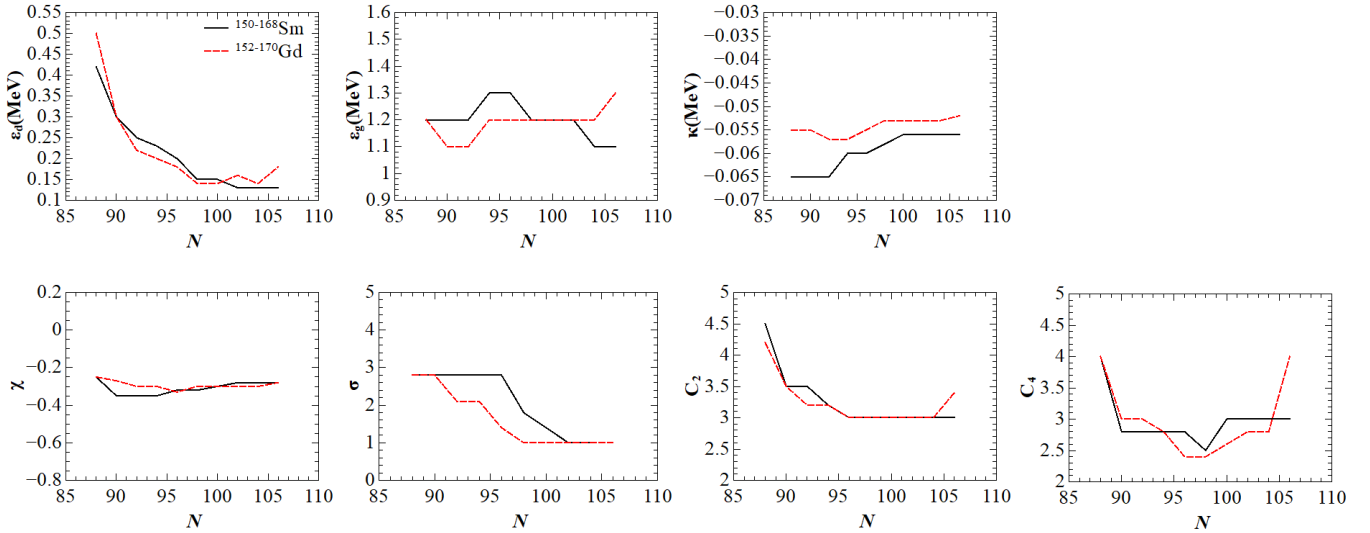


FIG. 5. Parameters of the *sdg* - IBM Hamiltonian Eq.(2), as functions of the neutron number N .

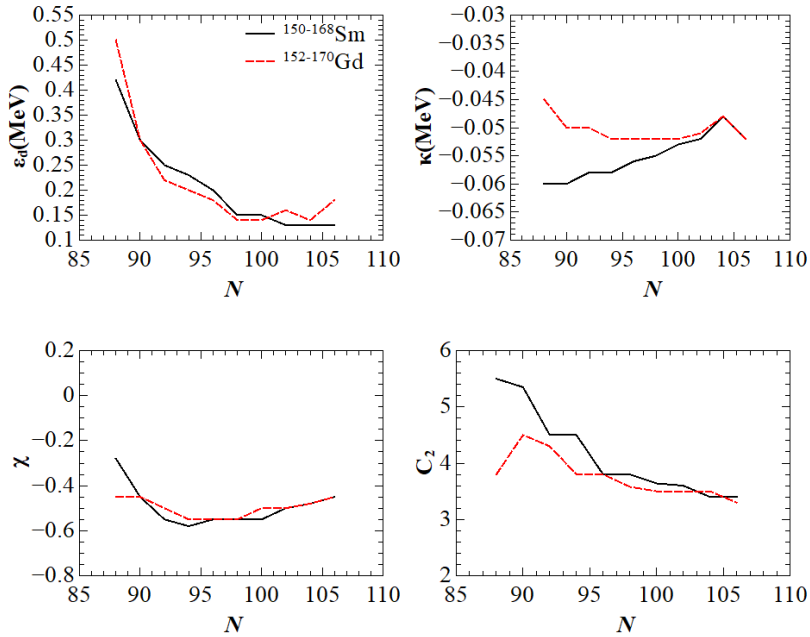


FIG. 6. Parameters of the *sd* - IBM Hamiltonian Eq.(6), as functions of the neutron number N .

stand whether the *sdg*-IBM describes them better.

3. Monopole transitions

Figure 12 shows the monopole strengths $\rho^2(E0; 0_i^+ \rightarrow 0_j^+)$, with $i = 2, 3$ and $j = 1, 2$, as functions of the neutron number N . In $N \leq 92$ isotopes, both models yield similar values of monopole strengths. As can be seen

from the figure, $\rho^2(E0; 0_3^+ \rightarrow 0_2^+)$ vanishes for $N > 92$. The *sdg*-IBM predicts a much sharper decrease (increase) of $\rho^2(E0; 0_2^+ \rightarrow 0_1^+)$ [$\rho^2(E0; 0_3^+ \rightarrow 0_1^+)$], with increasing neutron number, than the *sd*-IBM.

One can see from Figs. 12(a) and (c) that for those Sm and Gd nuclei with $N \geq 92$, the *sdg*-IBM predicts the monopole strengths $\rho^2(E0; 0_2^+ \rightarrow 0_1^+)$ and $\rho^2(E0; 0_3^+ \rightarrow 0_1^+)$ to be more or less similar to each other, whereas in the *sd*-IBM these monopole transition strengths are

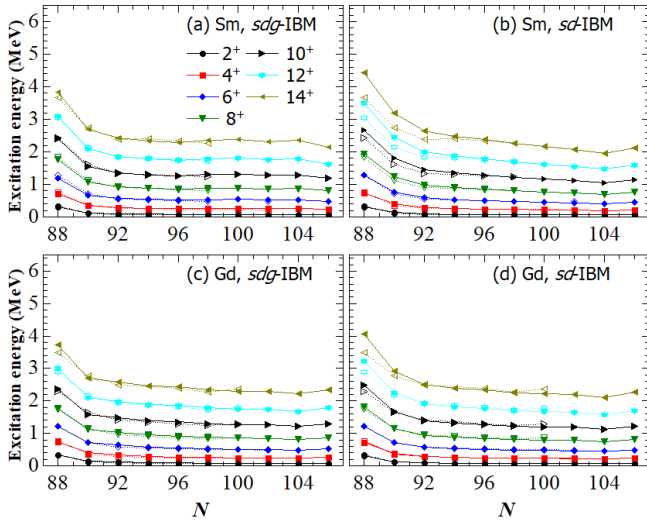


FIG. 7. Excitation energies of the yrast band states up to spin $J^\pi = 14^+$ as functions of the neutron number N within the mapped *sdg*-IBM (left column) and *sd*-IBM (right column), represented by solid symbols connected by solid lines. Experimental data are taken from Ref. [39], and are depicted as open symbols connected by dotted lines.

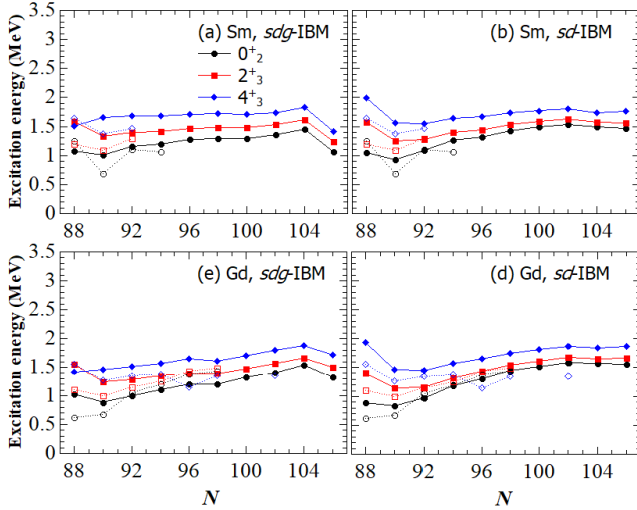


FIG. 8. The same as in Fig. 7, but for the excitation energies of 0_2^+ , 2_3^+ , and 4_3^+ states.

quite at variance, that is, the $\rho^2(E0; 0_2^+ \rightarrow 0_1^+)$ are larger than the $\rho^2(E0; 0_3^+ \rightarrow 0_1^+)$ by a factor of 2 to 3. In addition, the $\rho^2(E0; 0_2^+ \rightarrow 0_1^+)$ values obtained from the mapped *sdg*-IBM are smaller than those from the *sd*-IBM for neutron-rich nuclei with $N \geq 94$. The reduction of the $0_2^+ \rightarrow 0_1^+$ $E0$ transition in the case of the *sdg*-IBM has been already been discussed in Ref. [44]. On the other hand, the *sdg*-IBM provides larger $\rho^2(E0; 0_3^+ \rightarrow 0_1^+)$ values for the $N \geq 94$ nuclei than the *sd*-IBM. These

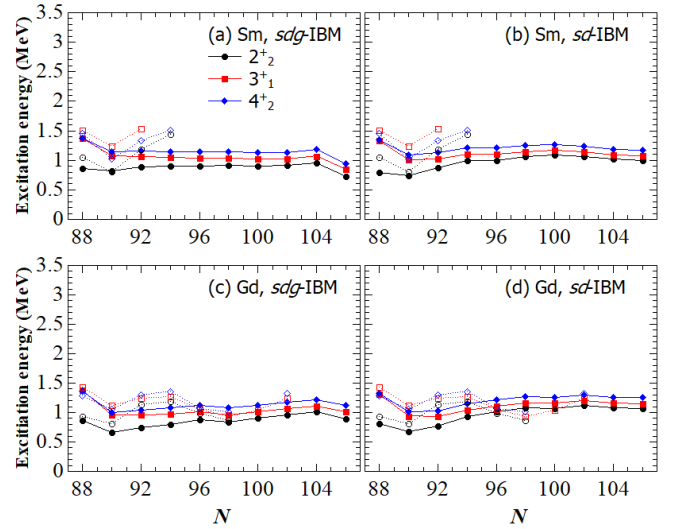


FIG. 9. The same as in Fig. 7, but for the excitation energies of 2_2^+ , 3_1^+ , and 4_2^+ states.

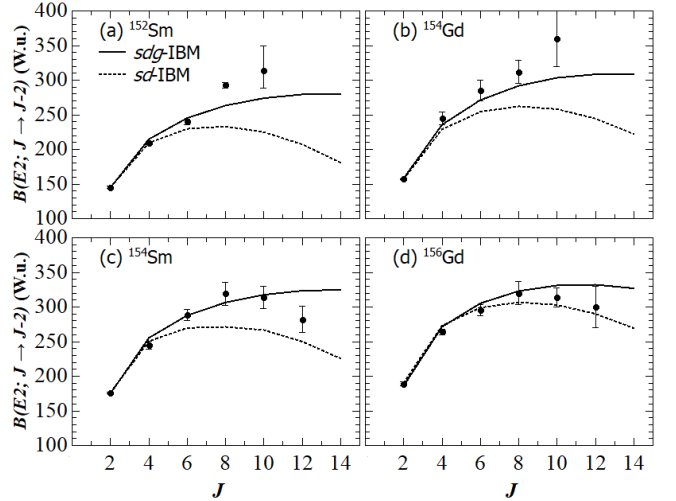


FIG. 10. $B(E2; J \rightarrow J-2)$ transition strengths in the ground state band of the well-deformed $N = 90$ (first row) and $N = 92$ (second row) isotopes as functions of spin J , computed with the mapped *sdg*-IBM (solid curves) and *sd*-IBM (dotted curves). The experimental data, represented by solid circles, are taken from Ref. [39].

quantitative differences in the predicted $\rho^2(E0)$ values between the two sets of the IBM calculations represent the most significant difference between the *sdg*-IBM and *sd*-IBM in the neutron-rich Sm and Gd isotopes with $N \geq 94$. As in the case of the hexadecapole transitions, experimental information about the monopole transitions is limited. It is therefore not possible to tell whether the *sdg*-IBM represents an improvement over the simpler *sd*-IBM in this respect.

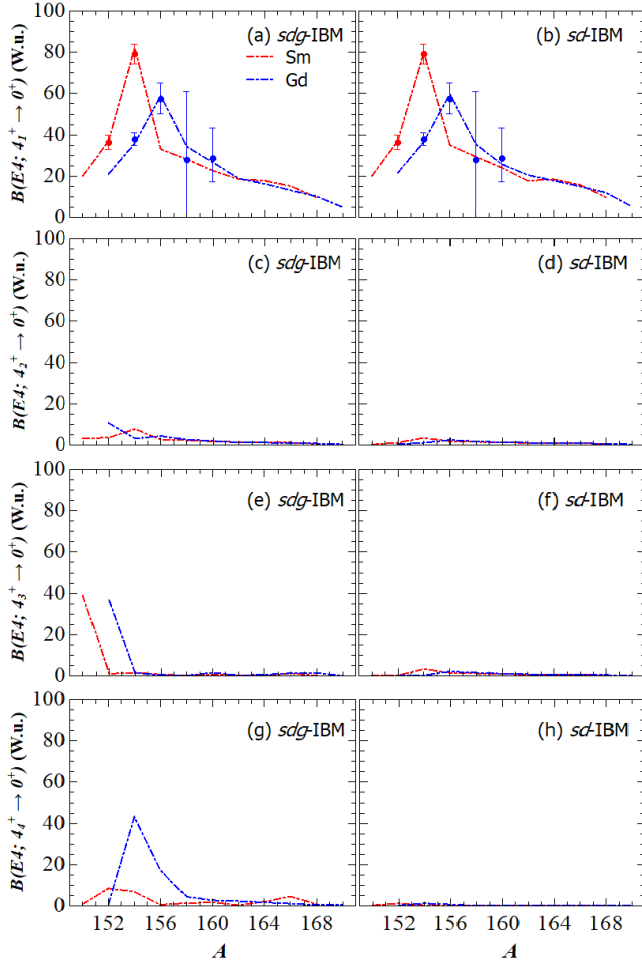


FIG. 11. $B(E4; 4_n^+ \rightarrow 0_1^+)$ ($n = 1, 2, 3, 4$) transition strengths as functions of the mass number A , computed with the mapped sdg -IBM (left column) and sd -IBM (right column). Experimental data, indicated by solid circles in the plots, are taken from Refs. [39, 46–48].

V. SUMMARY

We have presented an extensive analysis of the quadrupole-hexadecapole collectivity in even-even rare-earth isotopes $^{150-168}\text{Sm}$ and $^{152-170}\text{Gd}$, and the effects of hexadecapole correlations on low-lying excitation energies and transition strengths. The calculations were performed in the framework of the Gogny D1S EDF and the sdg -IBM and sd -IBM. The calculated results for the excitation spectra were shown to be in good agreement with the experimental data at the same level of accuracy as our previous mapped sdg -IBM studies based on the relativistic EDF [22, 23]. We have thus found that the quadrupole-hexadecapole mapping method does not significantly depend on the choice of the EDF.

The mapped sdg -IBM improves the description of the high-spin yrast states in the nuclei with $N = 88$, as well as in the Sm isotopes with $N = 90$ and 92. In heav-

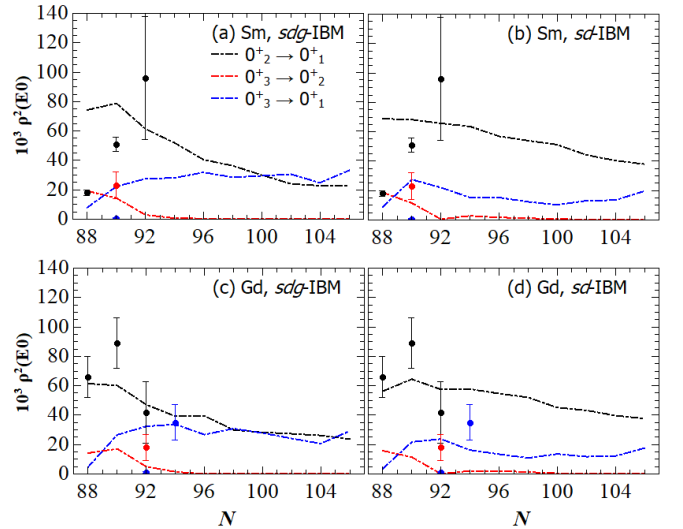


FIG. 12. $\rho^2(E0; 0_i^+ \rightarrow 0_j^+)$ values as functions of the neutron number N for Sm and Gd isotopes, computed with the mapped sdg -IBM (left column) and sd -IBM (right column). Experimental values, plotted as solid circles, are taken from Refs. [39, 49].

ier rare-earth nuclei, the contribution of g bosons to the ground state band is insignificant. In the case of the excited $K = 0^+$ and γ -vibrational bands, the sdg -IBM results did not differ significantly from the sd -IBM ones, with only some minor improvements of the 4_3^+ states of the $K = 0^+$ band at $N = 88$ in the sdg -IBM. In well-deformed $N = 90$ and 92 nuclei, the sdg -IBM predicts stronger $B(E2)$ transition strengths for the yrast states with spin $J^\pi \geq 6^+$, which is in good agreement with the experimental data. The effect is more visible in $^{152,154}\text{Sm}$, for which pronounced hexadecapole mean-field minima were found in the PESs. The choice of the Gogny D1S EDF seems to lead to somewhat stronger yrast band $B(E2)$ values compared to the ones obtained with the relativistic DD-PC1 EDF. The existence of the $K = 4^+$ band with an enhanced $B(E4; 4^+ \rightarrow 0^+)$ transition to the ground state is predicted by the sdg -IBM in ^{150}Sm and $^{152,154}\text{Gd}$. In heavier isotopes, such bands are also predicted, however, the bandhead in those nuclei is predicted to be a higher-lying $4_{n \geq 5}^+$ state. Regarding monopole strengths, the sdg -IBM predicts lower values of $\rho^2(E0; 0_2^+ \rightarrow 0_1^+)$ and larger values of $\rho^2(E0; 0_3^+ \rightarrow 0_1^+)$ in neutron-rich isotopes with $N \geq 94$, than the sd -IBM. This is in good agreement with previous theoretical calculations, and represents the most pronounced hexadecapole correlation effect on the low-lying spectra in very neutron-rich Sm and Gd isotopes. Due to the lack of experimental data on such transitions, it remains to be seen whether the sdg -IBM correctly predicts the behaviour of monopole transitions in those isotopes.

Now that the mapping method has been shown to be adequate for describing the quadrupole-hexadecapole col-

lectivity in nuclei, regardless of the choice of the EDF, the method can be extended to include even-odd and odd-odd nuclei. The method should also be applied to heavier rare-earth nuclei up to W and Os nuclei, where more experimental data on $E4$ transitions are available, and to explore possible hexadecapole correlations in other regions of the nuclear chart such as actinides. The method could also be extended to include proton and neutron degrees of freedom (i.e., *sdg*-IBM-2), which become relevant to describe phenomena like mixed-symmetry states and scissor modes.

ACKNOWLEDGMENTS

Most of the work by L.L. was done at the University of Zagreb and was funded within the Tenure

Track Pilot Programme of the Croatian Science Foundation and the École Polytechnique Fédérale de Lausanne, and the project TTP-2018-07-3554 Exotic Nuclear Structure and Dynamics, with funds from the Croatian-Swiss Research Programme. This work has also been supported by the Spanish Agencia Estatal de Investigación (AEI) of the Ministry of Science and Innovation (MCIN) under grant agreement No. PID2021-127890NB-I00. L.L. acknowledges support by the “Ramón y Cajal” grant No. RYC2021-031880-I funded by MCIN/AEI/10.13039/501100011033 and the European Union-”NextGenerationEU”. The work of R. Rodríguez-Guzmán was partially supported through the grant PID2022-136228NB-C22 funded by MCIN/AEI/10.13039/501100011033/FEDER, UE and ”ERDF A way of making Europe”.

-
- [1] A. Bohr and B. R. Mottelson, *Nuclear Structure*, Vol. II (Benjamin, New York, USA, 1975).
- [2] P. Ring and P. Schuck, *The Nuclear Many-Body Problem* (Springer-Verlag, Berlin, 1980).
- [3] Y. Gupta, B. Nayak, U. Garg, K. Hagino, K. Howard, N. Sensharma, M. Şenyiğit, W. Tan, P. O’Malley, M. Smith, R. Gandhi, T. Anderson, R. deBoer, B. Frentz, A. Gyurjinyan, O. Hall, M. Hall, J. Hu, E. Lamere, Q. Liu, A. Long, W. Lu, S. Lyons, K. Ost典iek, C. Seymour, M. Skulski, and B. Vande Kolk, *Phys. Lett. B* **806**, 135473 (2020).
- [4] W. Ryssens, G. Giacalone, B. Schenke, and C. Shen, *Phys. Rev. Lett.* **130**, 212302 (2023).
- [5] J. Chi, Y. Qiang, C. Gao, and J. Pei, *Nuclear Physics A* **1032**, 122626 (2023).
- [6] J. Engel and J. Menéndez, *Rep. Prog. Phys.* **80**, 046301 (2017).
- [7] F. Iachello and A. Arima, *The interacting boson model* (Cambridge University Press, Cambridge, 1987).
- [8] R. F. Casten and D. D. Warner, *Rev. Mod. Phys.* **60**, 389 (1988).
- [9] T. Otsuka, *Nucl. Phys. A* **368**, 244 (1981).
- [10] T. Otsuka, A. Arima, and N. Yoshinaga, *Phys. Rev. Lett.* **48**, 387 (1982).
- [11] T. Otsuka and J. N. Ginocchio, *Phys. Rev. Lett.* **55**, 276 (1985).
- [12] T. Otsuka and M. Sugita, *Phys. Lett. B* **209**, 140 (1988).
- [13] Y. D. Devi and V. K. B. Kota, *Z. Phys. A* **337**, 15 (1990).
- [14] S. Kuyucak, *Nucl. Phys. A* **570**, 187 (1994).
- [15] P. Van Isacker, A. Bouldjedri, and S. Zerguine, *Nucl. Phys. A* **836**, 225 (2010).
- [16] K. Nomura, N. Shimizu, and T. Otsuka, *Phys. Rev. Lett.* **101**, 142501 (2008).
- [17] K. Nomura, N. Shimizu, and T. Otsuka, *Phys. Rev. C* **81**, 044307 (2010).
- [18] K. Nomura, T. Otsuka, R. Rodríguez-Guzmán, L. M. Robledo, and P. Sarriguren, *Phys. Rev. C* **83**, 014309 (2011).
- [19] K. Nomura, N. Shimizu, D. Vretenar, T. Nikšić, and T. Otsuka, *Phys. Rev. Lett.* **108**, 132501 (2012).
- [20] K. Nomura, D. Vretenar, and B.-N. Lu, *Phys. Rev. C* **88**, 021303 (2013).
- [21] K. Nomura, D. Vretenar, T. Nikšić, and B.-N. Lu, *Phys. Rev. C* **89**, 024312 (2014).
- [22] L. Lotina and K. Nomura, *Phys. Rev. C* **109**, 034304 (2024).
- [23] L. Lotina and K. Nomura, *Phys. Rev. C* **109**, 044324 (2024).
- [24] D. Gogny, *Nuclear Physics A* **237**, 399 (1975).
- [25] J. Berger, M. Girod, and D. Gogny, *Nuclear Physics A* **428**, 23 (1984).
- [26] L. M. Robledo, T. R. Rodríguez, and R. R. Rodríguez-Guzmán, *J. Phys. G: Nucl. Part. Phys.* **46**, 013001 (2019).
- [27] S. Hilaire and M. Girod, *Eur. Phys. J. A* **33**, 237 (2007).
- [28] K. Nomura, R. Rodríguez-Guzmán, and L. M. Robledo, *Phys. Rev. C* **94**, 044314 (2016).
- [29] K. Nomura, R. Rodríguez-Guzmán, and L. M. Robledo, *Phys. Rev. C* **95**, 064310 (2017).
- [30] K. Nomura, R. Rodríguez-Guzmán, and L. M. Robledo, *Phys. Rev. C* **92**, 014312 (2015).
- [31] K. Nomura, R. Rodríguez-Guzmán, L. Robledo, and J. García-Ramos, *Phys. Rev. C* **103**, 044311 (2021).
- [32] K. Nomura, R. Rodríguez-Guzmán, L. M. Robledo, J. E. García-Ramos, and N. C. Hernández, *Phys. Rev. C* **104**, 044324 (2021).
- [33] K. Nomura, R. Rodríguez-Guzmán, and L. M. Robledo, *Phys. Rev. C* **104**, 054320 (2021).
- [34] C. V. N. Kumar and L. M. Robledo, *Phys. Rev. C* **108**, 034312 (2023).
- [35] B.-N. Lu, J. Zhao, E.-G. Zhao, and S.-G. Zhou, *Phys. Rev. C* **89**, 014323 (2014).
- [36] J. Zhao, B.-N. Lu, E.-G. Zhao, and S.-G. Zhou, *Phys. Rev. C* **95**, 014320 (2017).
- [37] T. Nikšić, D. Vretenar, and P. Ring, *Phys. Rev. C* **78**, 034318 (2008).
- [38] T. Nikšić, D. Vretenar, and P. Ring, *Prog. Part. Nucl. Phys.* **66**, 519 (2011).
- [39] Brookhaven National Nuclear Data Center, <http://www.nndc.bnl.gov>.

- [40] M. Warda, J. L. Egidio, L. M. Robledo, and K. Pomorski, [Phys. Rev. C **66**, 014310 \(2002\)](#).
- [41] J.-P. Delaroche, M. Girod, H. Goutte, and J. Libert, [Nuclear Physics A **771**, 103 \(2006\)](#).
- [42] V. K. B. Kota, J. V. der Jeugt, H. E. D. Meyer, and G. V. Berghe, [Journal of Mathematical Physics **28**, 1644 \(1987\)](#).
- [43] J. N. Ginocchio and M. W. Kirson, [Nucl. Phys. A **350**, 31 \(1980\)](#).
- [44] S. Zerguine, P. Van Isacker, and A. Bouldjedri, [Phys. Rev. C **85**, 034331 \(2012\)](#).
- [45] S. Heinze, computer program ARBMODEL, University of Cologne (2008).
- [46] R. M. Ronningen, J. H. Hamilton, L. Varnell, J. Lange, A. V. Ramayya, G. Garcia-Bermudez, W. Lourens, L. L. Riedinger, F. K. McGowan, P. H. Stelson, R. L. Robinson, and J. L. C. Ford, [Phys. Rev. C **16**, 2208 \(1977\)](#).
- [47] H. Wollersheim and T. W. Elze, [Nucl. Phys. A **278**, 87 \(1977\)](#).
- [48] R. M. Ronningen, R. B. Piercey, J. H. Hamilton, C. F. Maguire, A. V. Ramayya, H. Kawakami, B. van Nooijen, R. S. Grantham, W. K. Dagenhart, and L. L. Riedinger, [Phys. Rev. C **16**, 2218 \(1977\)](#).
- [49] T. Kibédi and R. Spear, [At. Data and Nucl. Data Tables **89**, 77 \(2005\)](#).